Electronic properties and photo-gain of UV-C photodetectors based on high-resistivity orthorhombic κ-Ga2O3 epilayers

Electronic properties and photo-gain of UV-C photodetectors based on high-resistivity orthorhombic κ-Ga_2O_3 epilayers

Carmine Borelli[(a)], Alessio Bosio[(a)], Antonella Parisini[(a)*], Maura Pavesi[(a)], Salvatore Vantaggio[(a)] and Roberto Fornari[(a,b)]

[(a)] *Dept. of Mathematical, Physical and Computer Sciences, University of Parma, Viale delle Scienze 7/A, 43124 Parma, Italy.*
[(b)] *Institute of Materials for Electronics and Magnetism (IMEM-CNR), Viale delle Scienze 37/A, 43124 Parma, Italy.*

* Corresponding author

Keywords: κ–Ga_2O_3, UV-C photodetector, responsivity, photodetector gain

Abstract

Electrical and optical properties of nominally-undoped high-resistivity κ-Ga_2O_3 epitaxial films are presented, along with the ultraviolet detection performance of solar-blind photodetectors fabricated from these epilayers. The photodetectors exhibited a solar-blind rejection ratio higher than 10^4, reproducible on-off switching times and a remarkable photo-gain (up to 10^3). The latter can be ascribed to either a strong trapping effect of *free holes* by deep levels inducing a majority carrier excess Δn with respect to the minority carriers Δp, or to a hole mobility several orders of magnitude lower than the electron mobility, both the hypothesis being consistent with literature data. A saturation of the gain, dependent on detector size, was observed beyond a certain applied voltage, that is consistent with a minority carrier diffusion length of a few 10^{-5} cm.
Non-critical growth conditions, reproducibility and intrinsic spectral selectivity together with good UV-detection performance make κ–Ga_2O_3 a suitable material for solar-blind ultraviolet photodetectors.

1. Introduction

Recently, solar-blind photodetectors (PD) for the C-range of the ultraviolet spectrum (UV-C) based on wide bandgap semiconductors have attracted great attention for their potential civil and military applications [1, 2, 3].
The ultraviolet (UV) radiation covers the wavelength range (400÷10) nm, commonly divided into four sub-ranges: UV-A (315 nm < λ < 400 nm), UV-B (280 nm < λ < 315 nm), UV-C (100 nm < λ < 280 nm) and extreme ultraviolet EUV (10 nm < λ < 120 nm) [4].
The sun radiates light over the entire UV spectrum, but the UV-C solar radiation is absorbed by atmospheric diatomic oxygen and by ozone, so that photons in the wavelength range 100 nm to 280 nm do not reach the ground. What reaches the Earth surface, in fact, is over 95% UV-A with a small contribution of UV-B.
Detectors exhibiting a cut-off below 280 nm are called solar-blind photodetectors, as no electrical signal is produced in daylight conditions.
Binary wide-bandgap semiconductors such as GaN [5], SiC [6] and ZnO [7] are in principle suitable for fabricating UV light detectors, but in order to meet the criteria of a solar-blind UV-C photodetector, external optical filters are required to prevent the longer wavelength from reaching the detector and generating photo-carriers. On the other hand, semiconductor ternary alloys with wider bandgap such as $Al_xGa_{1-x}N$ [8] and $Mg_xZn_{1-x}O$ [9] emerged as competitive technology for solar blind applications. However, these ternary

compounds suffer from phase segregation [10, 11], which introduces defects at the boundaries of discrete domains reducing the detection performance.

Recently, Ga_2O_3 attracted much interest for its unique advantages over other wide-bandgap semiconductors, including intrinsic UV-C spectral selectivity, high breakdown voltage and Baliga figure of merit. Furthermore, homoepitaxy is made possible by the availability of large Ga_2O_3 substrates, obtained from Czochralski or Edge-defined Film-fed Growth (EFG) single crystals. The melt growth of bulk Ga_2O_3, combined to easier epitaxial conditions for Ga_2O_3 than for the well-established nitride and silicon carbide semiconductors (lower deposition temperature and use of inexpensive O_2 or H_2O as one of the precursors), provide the precondition for a cost-effective oxide-based technology for optoelectronics and power electronics [12].

The Ga_2O_3 is known to have five polymorphs, labeled α, β, γ, δ, and κ. The monoclinic β-phase has been the focus of most research so far [12], as it is thermodynamically stable and can be prepared in form of single crystals [13] and thin films [14] .

However, β-Ga_2O_3 has a low symmetry structure (monoclinic) and presents anisotropic physical properties, as well as strong tendency to cleavage, which poses serious problems when going to device manufacturing.

For these reasons, there is an increasing interest about "novel" Ga_2O_3 polymorphs with more symmetric structure, among them the κ phase, with orthorhombic crystal lattice. It must be noted here, that the literature very often confuses the polymorphs ε and κ due to an initial misinterpretation of the six-fold diffraction patterns typical of such epitaxial films. Only later a very accurate TEM investigation revealed that this apparently hexagonal symmetry is actually produced by 120° rotational domains, all of them c-oriented with respect to the substrate [15].

The κ–phase offers the possibility of coupling a wide energy bandgap, similar to the β-one, with less critical epitaxial growth conditions, in particular an even lower deposition temperature. Although intrinsically metastable, no variations in the crystallographic structure of κ–Ga_2O_3 are observed up to about 700°C, whereas a complete conversion to the stable monoclinic β-phase occurs only above 900°C [16]. In the literature, only few articles [17-20] report information on the electrical, optical and photoelectrical properties of κ–Ga_2O_3: according to [18, 20] the room temperature (RT) bandgap is 4.7-4.8 eV while at low temperature the bandgap is about 5 eV [20]; not intentionally doped layers obtained by metal organic chemical vapor deposition (MOCVD) using Helium as carrier gas, exhibited RT resistivity values consistently higher than 10^7 Ωcm [18].

UV-C photodetectors based on κ–Ga_2O_3 could be integrated in solar-blind UV cameras for monitoring the corona discharge, a typical phenomenon that preludes failure of ceramic isolation in high voltage electrical systems, such as electrical transmission lines and power transformers [21]. Moreover, they may work as flame detector, for the early forest fire detection, as well as for anti-fire surveillance in high-risk facilities (powder silos, fuel transport, depot of explosive materials, etc…) [22].

Several PD based on β-Ga_2O_3 have been reported in the literature, mainly fabricated from heterojunctions [17].

In this work a thorough study of the UV photoresponse in resistive planar devices based on nominally undoped κ–Ga_2O_3 thin films is presented. In the discussion, the optical interaction between photons and active materials and the carrier transport processes are separately examined. In particular, the investigation has been focused on the dependence of the photo-gain on the applied bias for different electrode spacing. An estimate of the diffusion length of minority carriers is proposed, and an accurate evaluation of the rejection ratio is made by comparing the photoresponse under UV-C radiation with that at the whole sunlight radiation given by a solar simulator.

2. Experimental

Metal-semiconductor-metal (MSM) test structures were prepared on highly resistive nominally undoped κ–Ga_2O_3 thin films, similarly to preliminary experiments reported in [23]. The layers were grown by MOCVD on c-oriented Al_2O_3 substrates, using He as carrier gas. The epitaxial films had thickness of approximately 1 μm. and further details on the growth process were reported in [24]. X-ray diffraction (XRD) and SEM analysis

(not reported here) confirmed that the films were single phase with good morphology. Typical optical absorption data have previously been reported in Ref. [18], while details on the domain crystal structure of κ–Ga_2O_3 can be found in in Ref. [15].

Planar electrodes of SnO_x/ITO/Au [25] were sputtered on the surface of films through a stencil metal mask to fabricate four couples of contacts, differently spaced of L_1 = 0.2 mm, L_2 = 0.4 mm, L_3 = 0.8 mm, L_4 =1.6 mm, as shown in Fig. 1.

Each pair of adjacent contacts was biased in the range 0 ÷ 400 V by means of a Keithley Source-Meter Mod. 2400 (sensitivity 0,1 nA) while current-voltage curves (I-V) were recorded under monochromatic UV-C illumination (λ = 250 nm). The ohmic behavior of electrodes was reproducibly verified on a large number of films, confirming the robustness and reproducibility of the fabrication procedure.

The spectral photoresponse of these photoresistors was investigated by illuminating the free surface between adjacent contacts with a monochromatic light from an Oriel optical system consisting in a 250 W halogen lamp and a monochromator with wavelength resolution of 3 nm and spectral range 200 – 1000 nm. The spectral irradiance of the optical system was measured with a calibrated photodiode sensor (Newport 818 UV). Spectral responsivities were acquired at a fixed voltage of 200 V in the wavelength range 250 ÷ 650 nm.

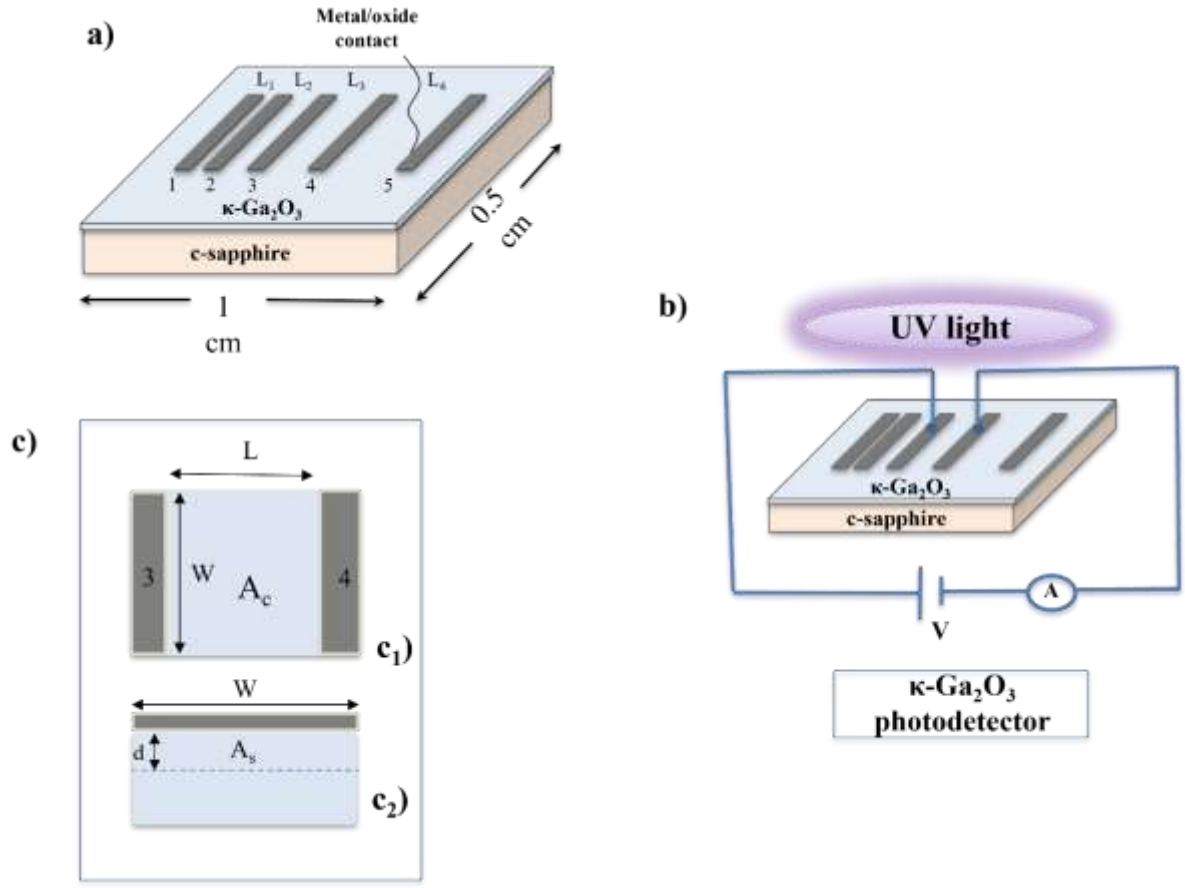

Fig.1: Schematic illustration of MSM test structures (**a**, **b**). Panel (**c**) shows the top view of the effective illuminated area $A_c = W \cdot L$ (**c**$_1$) and the cross section $A_s = W \cdot d$ (**c**$_2$ sketch), where L is the distance between two adjacent contacts, W is the contact length, and d is practically the thickness of the film in this case, as in principle it is twice the absorption length at the gap wavelength (see text for details).

The UV-C sensitivity of detectors was then evaluated by varying the irradiance from 40 μW/cm^2 to about 0,2 μW/cm^2 using neutral UV filters, and by testing stability and reproducibility of the transient photoresponse during on/off illumination cycles.
Finally, the effective solar blindness was tested comparing the photoresponse under sunlight with the UV-C photoresponse at 250 nm. Sunlight measurements were carried out using a solar simulator Oriel Mod. 81160-1000, designed to emit light with intensity and spectral composition similar to the natural sunlight, in AM 1.5 conditions. The solar blindness of photodetectors is quantified, as usual, by the rejection ratio UV/VIS, evaluated by the responsivity curve, that is appropriately corrected to normalize the response of the photodetector to a uniform spectral irradiance.

3. Results and discussion

a. Steady-state electro-optical characterization

It is known that the wide-bandgap semiconductor Ga_2O_3 presents a number of deep levels, which can influence the response times to light switch on/off in photodetectors made with this material [26]. It is therefore mandatory to have a precise acquisition of transient and steady-state physical quantities characterizing a PD test device. In the following, the achievement of the stationary regime has been accurately controlled with a tolerance on the measured value of 2% (50 ± 1 μA is the maximum value of measured current).
I-V curves acquired in the dark on a large number of MSM test structures showed an ohmic behavior up to 400V, in few cases associated to a moderate asymmetry of the characteristics for negative or positive voltage scans. The dark current at 200 V was 5 ÷ 10 nA, depending on the pair of contacts, indicative of the high resistivity of the layers. Low voltage measurements did not provide a measurable current as this was below the instrumental sensitivity.
The I-V curves under UV-C illumination (250 nm) on the other hand exhibited a good ohmic and symmetric behavior in the range ± (0÷400) V, with a significant photocurrent of few μA at 200V, as shown in Fig. 2(a) for a low irradiance of about 0,31 μW/cm^2. However, a slight non-linear trend at small voltages, in the range ± (1÷2) V, was observed as evidenced in the inset of Fig. 2(a). This behavior could probably derive from carrier trapping effects in the non-illuminated volume underneath electrical contacts. At low voltage, the flowing current is very low therefore the adjustment of spatial charge (related to traps) at the electrodes is very slow. The time required to reach the steady-state condition is longer the lower the applied voltage. At higher bias the contact region is crossed by tunneling [21] so that the stationary condition is reached rapidly, resulting in an ohmic regime of the current-voltage characteristics.
To check the sensitivity of κ–Ga_2O_3 to the UV-C radiation, photoresponse measurements under different 250 nm radiation fluxes were carried out. The trend in the Log-Log scale in Fig. 2(b) can be expressed as a power law with a slope equal to 1.09, confirming a good linear behavior in the range 0.37 ÷ 30.2 μWcm^{-2} and a wide range of detection capability of photodetector.
The responsivity *R* is the most important parameter to evaluate the real spectral selectivity of a photodetector and it is defined by:

$$R(\lambda) = \frac{I_{PC}}{P_{inc}(\lambda)} \qquad (1)$$

where I_{PC} is the measured photocurrent, i.e. the current under light with respect to the dark current at the same effective voltage, and P_{inc} is the incident optical power at a fixed wavelength on the effective illuminated area A_c of the sample.
The UV-to-VIS rejection ratio (R_R) is the most important figure of merit of UV-C solar-blind photodetectors. In the present work, R_R indicates the spectral selectivity of the device at λ = 250 nm with respect to λ = 500

nm and is defined as the ratio between the responsivity at λ = 250 nm (R_{250}) and the responsivity at λ = 500 nm (R_{500}): $R_R = R_{250}/R_{500}$. A value of R_R greater than 10^4 indicates a negligible photoresponse to visible light, which is a mandatory requirement for UV-C solar-blind detection [27, 28].

A typical responsivity spectrum of the investigated κ–Ga_2O_3 photodetector in the UV-VIS range is shown in Fig. 2(c). Marginal changes of the responsivity were observed upon change of the light intensity, as expected, whereas an always linear dependence of photocurrent on the light intensity was found in the investigated wavelength range.

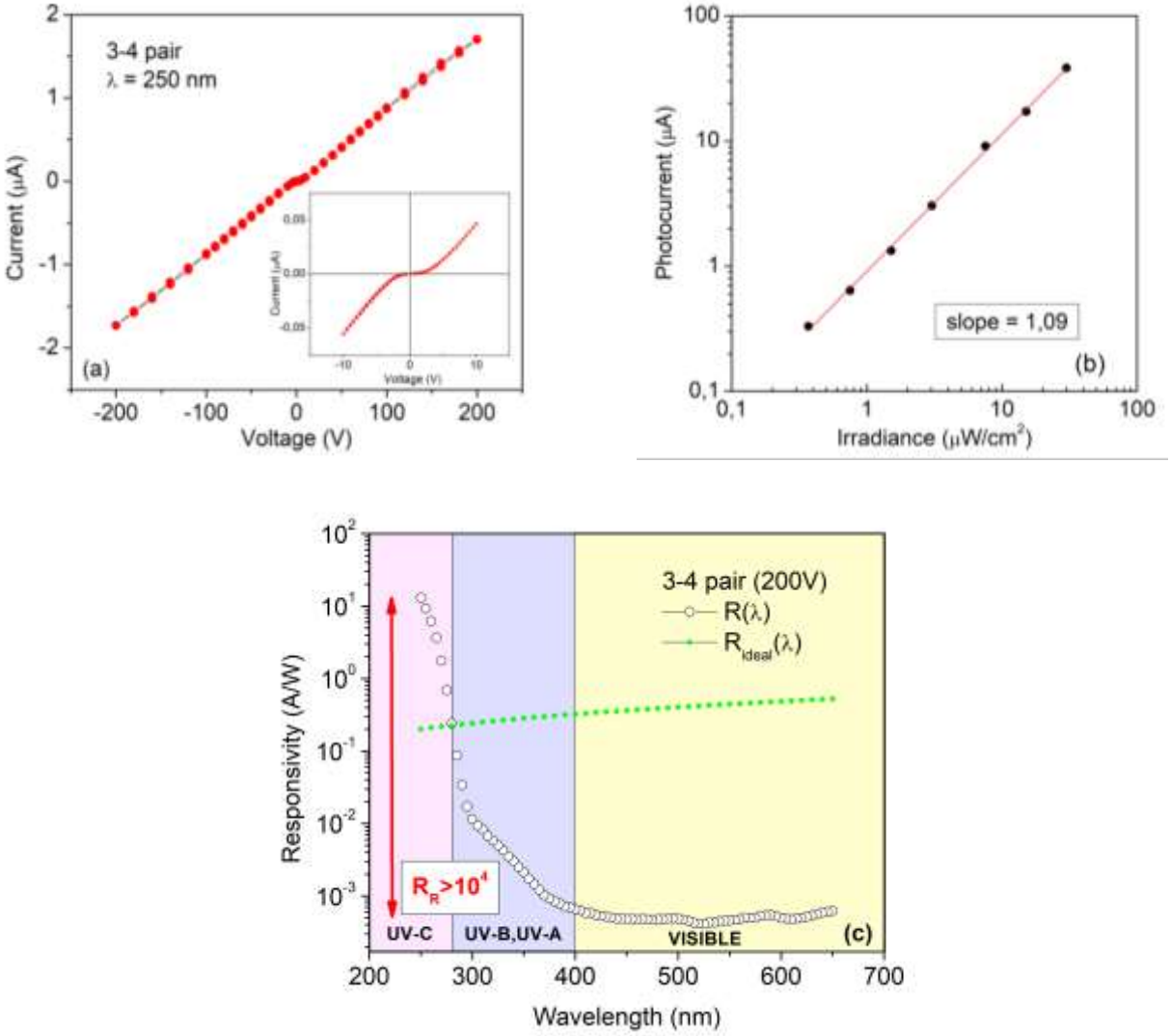

Fig. 2: (**a**) A typical I-V curve under UV-C illumination (λ = 250 nm), measured between the contacts 3-4. In the inset, the nonlinear trend of the photocurrent at low bias in the range ± (0÷10) V. (**b**) Photocurrent signal under UV-C light (λ = 250 nm) as a function of the irradiance at constant 200V bias. (**c**) Responsivity in the UV-visible region with 200 V applied to the 3-4 electrodes.

It is useful to express the responsivity in terms of the external quantum efficiency *EQE*. Remembering that the photo-gain *G* is defined as the ratio between the numbers of photogenerated carriers collected by the electrodes N_{el} and the number of absorbed photons $N_{ph,abs}$ [29] and introducing the entity $A(\lambda)=\frac{N_{ph,abs}(\lambda)}{N_{ph,inc}(\lambda)}$, the responsivity can be written as follows:

$$R(\lambda) = \frac{eN_{el}}{\frac{hc}{\lambda}N_{ph,inc}(\lambda)}\frac{N_{ph,abs}(\lambda)}{N_{ph,abs}(\lambda)} = \frac{\lambda e}{hc}\cdot A(\lambda)G(\lambda) = R_{ideal}(\lambda)\cdot EQE(\lambda) \qquad (2)$$

where λ is the wavelength of the incident radiation, h is the Planck constant, c is the speed of light, e is the electron charge and the product $A(\lambda)G(\lambda)$ is the external quantum efficiency.
The photo-gain G measures the carrier collection efficiency of the detector with respect to the density of incident photons, thus it strongly depends on recombination rate of photocarriers prior to collection at the electrodes. $A(\lambda)$ is related to the absorbance, which takes into account of the effective number of photons absorbed by the active layer of the detector, hence it provides the number of free carrier pairs generated inside the active volume of the photodetector. If *EQE = 1*, i.e. in the ideal case of all photogenerated hole-electron pair collected at the electrodes, the responsivity for 250 nm photons should be R_{ideal} = 0,21 A/W.
Fig. 2c shows the spectral responsivity of a representative MSM test structure together with the ideal responsivity calculated at different wavelengths (green line). It is important to note that in the UV-C region the responsivity of the photodetector overcomes its ideal value: the photo-gain reaches values higher than the unit, whereas the responsivity remains well below its ideal value in the visible region. The understanding of this fact requires an analysis of photoconduction mechanisms, taking into account the transport properties of gallium oxide.

b. Analysis of photo-gain

Starting from Eq. (2), the photo-gain G can be written as:

$$G = \frac{N_{el}}{N_{ph,abs}} = \frac{R}{A(\lambda)\cdot R_{ideal}} = \frac{hc}{A(\lambda)\cdot e\lambda}\frac{J_{ph}\cdot A_s}{P_{inc}} \qquad (3)$$

where J_{ph} is the photocurrent density flowing across the cross section of the film $A_s = W\cdot d$, with W the contact length and d the thickness within which light is totally absorbed (see Fig. 1), generally estimated as about 2 times the radiation absorption length, then in our case it is comparable to the layer thickness.
The evaluation of gain is of interest at the wavelength of the responsivity maximum, in our case at 250 nm.
It is important to note that the entity $A(\lambda)$ could be much different from the unit if reflectance and transmittance of the film are not negligible (in the present discussion the reflections from the interface with the substrate is neglected). Transmittance, generally depends on the film thickness and on the radiation wavelength; however, in the UV-C region, where the gain is evaluated, a value of absorption coefficient for κ–$Ga_2O_3 > 10^4$ cm^{-1} was reported [18]; therefore we are confident that the entire incident light at 250 nm is fully absorbed within the epilayer thickness.
Introducing the carrier generation rate g, i.e. the number of free carriers generated per second in the unit volume:

$$g = \frac{P_{inc}}{V_{gen}}\cdot\frac{\lambda}{hc} \qquad (4)$$

where $V_{gen} = A_c\, d = WLd$ is the volume of layer that contributes actively to the photocurrent. The gain then becomes:

$$G = \frac{J_{ph}\cdot W\cdot d}{eg(WdL)} = \frac{J_{ph}}{geL} \qquad (5)$$

and J_{ph} can be written, from the classical theory, in terms of electron and hole mobility, μ_n and μ_p respectively, concentration of photo-generated carriers Δn and Δp and electric field E:

$$J_{ph} = e\left(\mu_n \Delta n + \mu_p \Delta p\right) \cdot E \qquad (6)$$

Let us consider a high-resistivity *n*-type semiconductor, as is the case of κ–Ga_2O_3. Under uniform illumination and low-injection conditions, absorbed photons generate an excess of electron-hole pairs that is uniform in space and independent of the applied electric field. The densities of both kinds of photo-carriers are equal and regulated by the recombination rate of minority carriers, so that $\Delta n = \Delta p = g \cdot \tau_p$, where τ_p is the mean lifetime of the holes. The expression for *G* thus becomes:

$$G = \frac{\tau_p \mu_p E}{L}\left(1 + \frac{\mu_n}{\mu_p}\right) = \frac{\tau_p}{\tau_t}\left(1 + \frac{\mu_n}{\mu_p}\right) \qquad (7)$$

here $\tau_t = L/(\mu_p \cdot E)$ represents the transit time for holes under uniform electric field. This is the classic expression of the gain *G* in an ideal *n*-type photoconductor, which exhibits a linear dependence from the electric field. According to Eq. (7), in order to increase the gain one can reduce the transit time increasing the electric field and/or reducing the contact spacing. Extremely high values of *G* (up to $10^3 \div 10^5$) measured in Ga_2O_3 MSM photodetectors [30] are not conceivable in the frame of the classical theory, neither as result of avalanche phenomena because the applied electric field does not overcome $10^3 \div 10^4$ V/cm.
This observation makes questionable the applicability of Eq. (7) and imposes a careful analysis of assumptions made for its derivation:

1. homogeneously doped *n*-type semiconductors.
2. lifetime $\tau_p = \tau_n$, i.e. photo-generation rate is low (low-injection conditions), so that the electrical transport is ruled by minority carriers;
3. excess of photo-generated free carriers $\Delta n = \Delta p = g\tau_p$, which is strictly true only if Δp and Δn are uniformly distributed in space and constant in time;
4. the internal electric field is assumed to be uniform;
5. trapping effects are neglected.

It is important to observe that in a purely resistive photoconductor with a planar MSM geometry (ohmic contacts) a non-uniform carrier distribution is always expected at the electrode edges, where the illuminated part of detector is adjacent to the shaded region underneath the metal contacts (see Fig. 3). This effect is expected to be enhanced in a highly resistive material such as κ–Ga_2O_3 (generally dark-resistivity $\rho > 10^7$ Ω·cm) [31]. Nevertheless, Eq. (7) can still be considered valid at zero or low bias, when the non-uniformity of the concentrations of photo-carriers is confined in proximity of the contacts (Fig. 3a). In this case, the assumption $\Delta p = g \cdot \tau_p$ may be considered as valid [32] and a linear increase of gain with the applied bias is expected, maintaining anyway values around unity.
On the other hand, a deviation from this linear behavior takes place when the spatial non-uniformity of the minority carrier density increases with electric field magnitude, as predicted by the continuity equation for minority carriers in stationary conditions, and it affects a wide region away from the contacts, extending deeply into the conductive channel (Fig. 3b). In fact, for electric fields lower than the critical value $E_c = K_B T/eL_{Diff,p}$, where K_B is the Boltzmann constant and $L_{Diff,p}$ the minority-carrier diffusion length (in a n-type semiconductor), the diffusive processes mainly dominate the minority carrier transport [33].

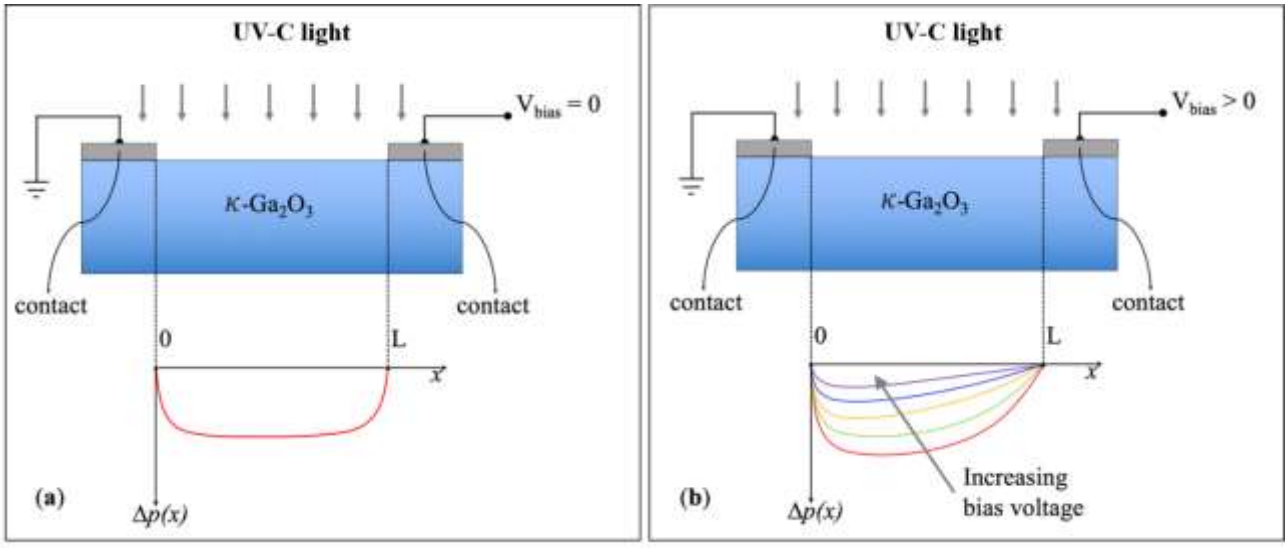

Fig. 3: Qualitative distribution of photo-generated holes $\Delta p(x)$ between ohmic contacts under uniform illumination with UV-C radiation: (**a**) no bias applied; (**b**) with bias applied.

For electric fields significantly higher than E_c, the $\Delta p(x)$ profile is mainly controlled by the drift processes through the drift length $L_{Drift} = \mu_p \tau_p E$. In this limit, the expression $\Delta p = g \cdot \tau_p$ (or $\Delta n = g \cdot \tau_n$) of spatially independent excess carriers, used to derive Eq. (7), is no longer valid and a saturation of gain is expected, but anyway with values around unity [32]. Therefore, Eq. (7) becomes inadequate to describe the photoconductivity at high electric fields, as well as the high values of gain experimentally observed.
The physical nature of the gain (especially when G>>1) is still matter of debate: in Ref. [32] it was suggested that in a real semiconductor, when carrier trapping is not negligible, the assumption $\Delta p = \Delta n$ is no longer valid, and the concentration of collected carriers in Eq. (6) differs from the initial concentration of photo-generated carriers.
Let us define more precisely the situation of our photodetectors:

1) In presence of a high optical injection, each of the two carrier species exceeds its equilibrium concentration, a condition easily obtained in highly resistive materials such as nominally undoped Ga_2O_3.

2) Photocarriers are always generated in pairs, but when trapping phenomena are present for one type of carrier, the two species can be collected at the electrodes with different rates, therefore, in these conditions $\Delta n \neq \Delta p$.

3) The known phenomenon of hole self-trapping [34] could indeed justify the hypothesis $\Delta n > \Delta p$; moreover, also hole trapping by deep levels might be effective, as demonstrated for the βpolymorph [35, 36]

For these reasons, starting again from Eq. (5) and Eq. (6) an equation similar to Eq. (7) can be obtained by defining the ratio $\gamma = \Delta n / \Delta p$ between the different concentrations of the two species of photocarriers, with γ greater than unit.
In the limit of low electric field, Eq. (7) can be re-written as (see also Ref. [32])

$$G = \frac{\tau_p}{\tau_t}\left(1 + \gamma \cdot \frac{\mu_n}{\mu_p}\right) \qquad (8)$$

This new formula can justify the high experimental values of gain, because of $\gamma > 1$ and $\mu_n >> \mu_p$. Eq. (8) is valid if γ is constant and uniform across the detector, but such condition is probably not met because of electrodes. Furthermore, the system under constant illumination is stationary but strongly off-equilibrium.

To take these considerations into account, average constant values can be introduced $\Delta p(x) = \Delta p_{avg} \neq \Delta n(x) = \Delta n_{avg}$ as long as the non-uniformity of the electric field is weak, together with an effective mean lifetime $\tau_{p,eff}$ for holes so that $\Delta p_{avg} = g \cdot \tau_{p,eff}$. Eq. (8) then becomes:

$$G = \frac{\tau_{p,eff}}{\tau_t}\left(1 + \gamma \cdot \frac{\mu_n}{\mu_p}\right) \qquad (9)$$

which substitutes Eq. (7) in low field limit ($E < E_c$), again consistent with a linear dependence of gain on applied voltage.
A simple view of how traps can induce high gain is as follows: under stationary illumination, a constant density N_t of photogenerated holes is trapped (or self-trapped), an equal density of photogenerated free electrons must be maintained in the semiconductor to guarantee the local charge neutrality. Hole traps are likely filled during the transient at the beginning of the sample illumination, up to reaching a stationary state after which light will continue to generate equal amounts of free electrons and free holes, $g\tau_{p,eff}$. The applied bias will drive the free carriers to the electrodes and allow for collecting *on average* $\Delta p = g\tau_{p,eff}$ free holes (not all the photogenerated holes are trapped) and $\Delta n = g\tau_{p,eff} + N_t$ free electrons. Such mechanism explains the relation $\Delta n > \Delta p$ and, consequently, the more significant the hole trapping the higher the γ value.
The experimental photo-gain at fixed light power shows three different trends as a function of applied voltage (Fig. 4):

1) very low bias voltages: the system does not reach easily a stationary condition, as said before in the discussion about I-V curves, and *G* is lower than unit up to 2.5 V between the couple of contacts 1-2 (inset in Fig. 4a) and up to 10 V for contacts 3-4 (inset in Fig. 4b);

2) intermediate bias voltages: *G* shows a linear behavior as predicted by Eq. (9), which suggests an almost uniform distribution of minority carrier excess $\Delta p(x)$ far from the contacts, thus only weakly influenced by the electric field. The depletion region close/under the contacts, where photocarrier concentration drops to zero, is narrow enough to allow the tunneling of photoelectrons without affecting the photocurrent signal. Hole self-trapping and hole trapping are anyway effective and responsible for the high values of gain. This bias extends up to about 150 V for the closest contacts and up to about 250 V for contacts 3 - 4.

3) At even higher bias the off-equilibrium $\Delta n(x)$ and $\Delta p(x)$ are strongly space dependent. The carrier density profiles as well as their lifetimes differ considerably along the photoconductive channel between the electrodes, which leads to building an internal electric field. The photo-generated carriers feel an effective electric field arising from the overlap of the external bias and the built-in field. In this case, *G* tend to saturate and because of trapping, its value is much higher than unity [32].

In Fig. 4b the three regions described above are still evident, but the saturation of the gain starts at higher bias, as expected since $L_{3\text{-}4} = 4\,L_{1\text{-}2}$. The maximum gain *G* obtained with the contact pair 3-4 is about four times less than that obtained with the pair 1-2; therefore, it scales with the distance between the couples of contacts and with the external bias.

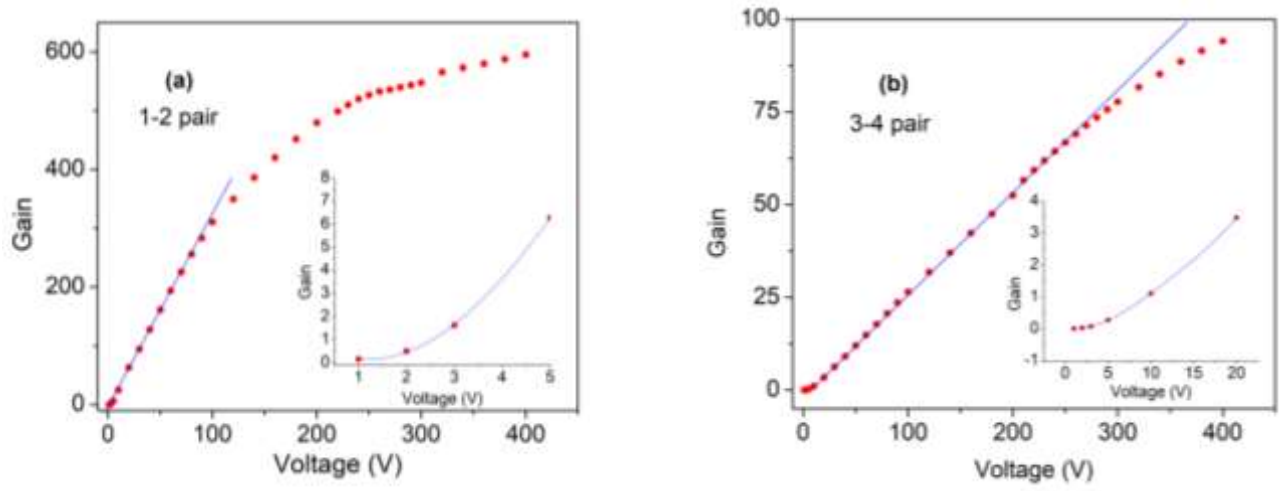

Fig. 4: Photoelectric gain *G* as a function of voltage applied to 1-2 (**a**) and 3-4 (**b**) contact pairs for incident 250 nm photons. Insets represent the gain behavior at very low voltage.

The same linear dependence of the gain on the applied voltage shown by Fig. 4a was obtained by acquiring the spectral responsivity at different voltages, normalizing them to the ideal responsivity R_{ideal} = 0,21 A/W and taking the value at the wavelength of 250 nm for each applied bias, as Fig. 5 shows. The responsivity measurements were carried out using the contact pair 3-4, at different bias under UV light in the wavelength range of (250÷300) nm (Fig. 5a). The photo-gain as a function of the bias applied to the same pair 3-4 is reported in Fig 5b. The voltage range corresponds to the linear behavior of the plot of Fig. 4b, with a maximum gain of about 50, lower than that revealed for the pair 1-2 (Fig. 4a). This is mainly due to the higher transit time, although a different voltage partition between conductive channel and contact regions in 1-2 pair with respect to 3-4 pair cannot be excluded. This comparison demonstrates that the timing in the acquisition of the spectral responsivity curves is slow enough to enable stationary conditions at any step of the measurement, and the same conclusion is true when the gain is measured by varying the applied voltage, i.e. the gain is independent of the acquisition method, which also guarantees a reproducible behavior of the contacts under polarization.

The different slopes of the linear trends in Figs. 4 are justified by the different resistances of the two conductive channels by virtue of their different lengths. The contacts do not play a significant role except in the very low voltage regimes. Under this hypothesis, gain saturation can thus be interpreted as a consequence of the high field conditions i.e. $E >> E_c$. In this frame, an estimate of hole diffusion length $L_{D,p}$ and excess photo-carrier factor γ can be obtained.

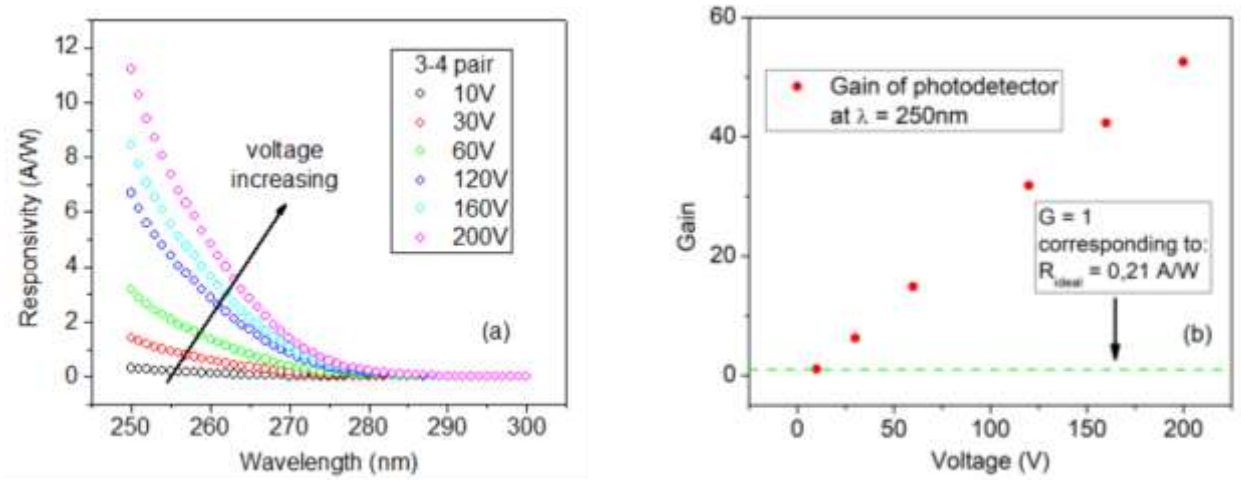

Fig. 5: (**a**) Responsivity in the wavelength range (250÷300) nm; the increasing voltage was applied between contacts 3 and 4. (**b**) Photo-gain (G) and as a function of the applied voltage under radiation with λ = 250 nm. The dashed green line denotes the theoretical value of photo-gain G = 1 at λ = 250 nm (R_{ideal} = 0.21 A/W).

c. Diffusion length

Let us consider the voltage at which the gain starts deviating from linearity: it is about 100 V in case of pair 1-2 and about 300 V in case of pair 3-4, corresponding to an electric field E_t of about 5 kV/cm and about 4 kV/cm, respectively. To obtain a correspondence between such E_t values and E_c, we compare these data with the results of the analysis proposed in [26], although that calculation was for p-type silicon and no trapping effects was considered. In that reference, the departure from the linear trend of the photocurrent occurred at about $E_t = 0{,}8$ KV/cm.

The minority carrier diffusion length can be evaluated from the relation $L_{D,min} = \sqrt{\mu_{min}\tau_{min}K_BT/e}$, where the Einstein relation ($D_{min} = \mu_{min}K_BT/e$) between diffusion coefficient and mobility is applied, τ_{min} and μ_{min} are respectively lifetime and mobility of the minority carriers (the holes *p* in our case). Data reported in [32] permit to observe that, at RT, E_c was about 5 times lower than E_t. If this ratio is assumed equally valid for our samples, by neglecting non-uniformity of the electric field due to traps, a rough value of E_c can be estimated for our samples, which should be about 1 kV/cm, leading to a RT hole diffusion length of $L_{D,p} = (2.5 \div 3.5) \times 10^{-5}$ cm. This range of values accounts well for both sets of data of Figs. 4. Although affected by uncertainty, this is the first estimate of diffusion length for the ε phase and is remarkably consistent with values reported for the β phase [37].

Taking such diffusion length and the slope of photo-gain as a function of voltage (Figs. 4), one can evaluate the ratio γ, which provides an estimate of hole trapping/self-trapping magnitude. In the linear region, i.e. for E < E_c, the gain in Eq. (9) can be rewritten in terms of $L_{D,p}$ by considering the relation $L_{D,p} = \sqrt{D_p\tau_{p,eff}}$, the Einstein relation $D_p = \mu_p KT/e$ and the definition of transit time:

$$G = \frac{L_{D,p}^2}{L^2}\frac{e}{K_BT}\left(1 + \gamma \cdot \frac{\mu_n}{\mu_p}\right)V \qquad (10)$$

Considering that the slopes *m* of the linear parts of the plots in Fig 4a and 4b are about 3 V^{-1} and 0.25 V^{-1}, respectively, and scale as L^2, one finds that the product mL^2 assumes the same value for both plots. It is thus possible to write the following relation for any arbitrary slope *m*:

$$mL^2 = L_{D,p}^2 \frac{e}{KT}\left(1 + \gamma \cdot \frac{\mu_n}{\mu_p}\right) \quad (11)$$

The experimental slopes and the evaluated $L_{D,p}$ at RT can be inserted in Eq. (11) to estimate the product $\gamma \cdot \mu_n/\mu_p$.

As no reliable data about hole trapping and/or self-trapping in κ–Ga_2O_3 is available, we shall consider two limit cases: (i) negligible self-trapping and (ii) total self-trapping of photo-excited holes. In case (i), a fraction of photoexcited holes must be trapped in deep levels, whereas the residual photoholes are assumed to be free (the collected Δp). In this case, the ratio of free carrier mobility μ_n/μ_p can be estimated considering the carrier interaction with optical phonons as dominant scattering mechanism at RT, similarly to what observed for the beta phase [38]. The mobility ratio can thus be obtained from the electron and hole effective masses $\mu_n/\mu_p = \left(m_p/m_n\right)^{1.5} \sim 52.4$, where $m_p \sim 4.2m_0$ [39] and $m_n \sim 0.3m_0$ [40] are the estimated hole and electron masses in κ-Ga_2O_3, with m_0 the standard rest electron mass. Hence, the γ ratio would be about 10^3, which means that the density of collected photoelectrons per unit of time would be about 10^3 times bigger than that of collected photoholes.

In case (ii), the total self-trapping would be responsible for the photo-gain in the resistive κ–Ga_2O_3 detector. This means that the concentrations of the two photocarriers are equal, but the photogenerated holes are practically immobile. In the limit of $\gamma = 1$, Eq. (11) gives a mobility ratio $\mu_n/\mu_p \sim 1{,}2 \times 10^6$, which corresponds to a mobility of the self-trapped holes of about 1×10^{-6} cm^2/Vs if an electron mobility of a few cm^2/Vs is considered.

In conclusion, the high photo-gain observed in our photo-resistor may be explained either by a low concentration of free photoholes with fairly good mobility (effective hole trapping by deep levels and $\gamma >> 1$) or by a total hole self-trapping that kills their mobility (effective hole self-trapping and $\gamma \sim 1$). Intermediate/mixed cases are conceivable as well. At the present stage of knowledge, we may not state which of the above situations better accounts for the measured photo-gain. Interestingly, there is still much uncertainty on the actual hole mobility in β-Ga_2O_3: in a simulation work about Schottky PD, Akyol estimated a *non-equilibrium* hole mobility of about 20 cm^2/Vs [41], while according to Varley et al. [42] the *self-trapped* hole mobility is seven orders of magnitude lower.

d. Transient photoresponse

To evaluate the stability and performance of the photodetector, the photoresponse was recorded during ON-OFF photoexcitation cycles. Fig. 6 shows the photocurrent transient under UV-C radiation at λ = 250 nm and applied voltage of 200V. Both rise and the decay times of the photocurrent signal were analyzed by means of a bi-exponential analytical curve, taking two different time constants:

$$I(t) \propto I_0 + exp\left(-\frac{t}{\tau_1}\right) + exp\left(-\frac{t}{\tau_2}\right) \quad (12)$$

where I_0 is the dark current, τ_1 represents the fast time constant while τ_2 is the slow time constant.

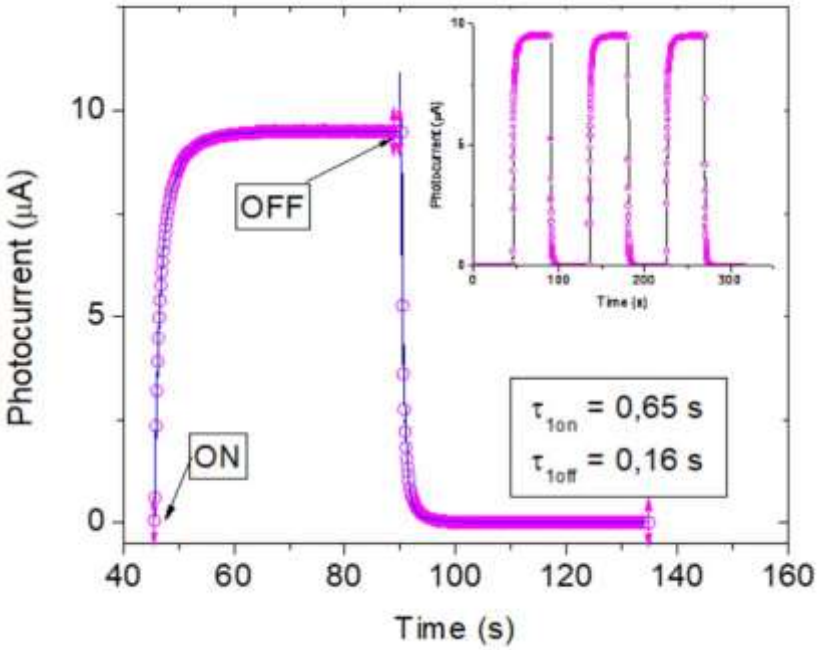

Fig. 6: Time-dependent photoresponse: experimental curve (circles) and fitted curve (solid line) of the current rising and decay processes under 250 nm illumination (I = 16 μW/cm^2) for pair 3-4 at V = 200V. In the inset: repeated cycles on/off show that photodetector maintains stability.

Table 1: Photocurrent rise and decay times refer to the 3 cycles on/off shown in the inset of the Fig.6.

ON/OFF CYCLES	τ_{1on} (s)	τ_{2on} (s)	τ_{1off} (s)	τ_{2off} (s)
I	0,65	2,59	0,16	1,21
II	0,69	2,99	0,34	1,85
III	0,68	3,03	0,29	1,57
Average	**0,67**	**2,87**	**0,26**	**1,55**

In our case, τ_{1on} and τ_{1off} were found to be around 0.7 s and 0.3 s, respectively, which are comparable to those previously reported for different types of photodetectors based on different phases of Ga_2O_3 (Table 2). We note that the performance of the ohmic MSM devices reported in Table 2 depends on the distance between electrodes, because the smaller the spacing the more efficient is the charge collection. Therefore, due to the different geometries of the devices listed in Table 2, a quantitative comparison is not possible. We must observe that the results of the present work refer to a device with contact distance of 800 μm while in other cases of Table 2 it is smaller. This is an important experimental detail to be considered when comparing the data of Table 2.

Note that the photocurrent profile remained unchanged after several ON-OFF switching cycles (inset of Fig. 6), which demonstrates good stability and reproducibility.

To prove that κ–Ga_2O_3 is suitable for use in daylight conditions, additional measurements with a solar simulator were carried out. The goal of this analysis was to prove the solar-blind character of the device, taking into account the radiation actually impinging on the detector.

In the literature, the rejection ratio is often defined as $R = \frac{R_{UVC}}{R_{500}}$, that is the responsivity ratio at just two reference wavelengths, namely 250 nm and 500 nm. However, since the device must be blind against the global

sunlight, it is more meaningful to take the photocurrent, and consequently the responsivity, of the entire visible spectrum.

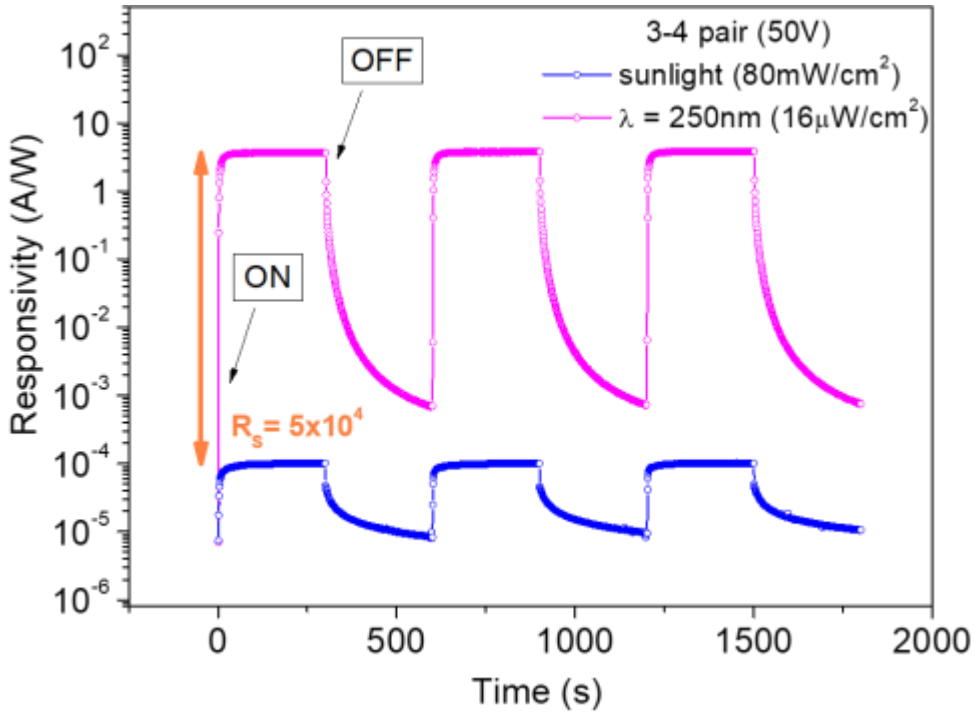

Fig. 7: Time-dependent photoresponse (Log scale) under two illumination conditions (λ = 250 nm and sunlight exposure). The rejection ratio R_S greater than 10^4 confirms the excellent solar-blind features.

In these tests, the power density of the solar simulator (I = 80 mW/cm^2), was over three orders of magnitude higher than that of the UV-C radiation from the halogen lamp (I = 16μW/cm^2). Nevertheless, as shown in Fig. 7, the photoresponse from UV-C light at 250 nm is by far stronger than the one from background solar light. The contribution of solar radiation can be calculated as follows:

$$R_{SUN} = \frac{\int_{400}^{700} f(\lambda)R(\lambda)d\lambda}{\int_{280}^{4000} f(\lambda)d\lambda} \qquad (13)$$

where $R(\lambda)$ is the spectral responsivity of the photodetector, in $\left[\frac{A}{W}\right]$, and $f(\lambda)$ is the spectral irradiance of the solar simulator, in $\left[\frac{W}{cm^2 \cdot nm}\right]$.

Considering that $R_{UVC} = 3{,}5\ \left[\frac{A}{W}\right]$ and $R_{SUN} = 0{,}7 \times 10^{-4}\ \left[\frac{A}{W}\right]$, an UV/sunlight rejection ratio R_S of 5×10^4 can be derived, which confirms the excellent solar-blind performance of our photodetectors based on undoped κ–Ga_2O_3.

Table 2: Comparison between basic parameters of representative Ga_2O_3 UV photodetectors based on a MSM device structure.

Ga_2O_3	Structure	Responsivity [A/W]	Rejection Ratio	τ_{rise} (s)	τ_{decay} (s)	Reference
κ	Ohmic MSM (SnO_x+ITO+Au)	**11 (at 200V; spacing 800 μm)**	**> 10^4**	**0.7**	**0.3**	**This work**
β	Ohmic MSM (Ti/Au)	- (spacing 200 μm)	-	0.86	1.02	[27]
β	Ohmic MSM (Ti/Au)	259 (at 20V; spacing 3 μm)	1×10^2	0.1	2.1	[45]
β	Ohmic MSM (Ti/Au)	8.41 (at 10V; spacing 5 μm)	3.2×10^3	2.97	0.41	[46]
β	Ohmic MSM (Ti/Al)	54.9 (at 20V; spacing 5 μm)	3.2×10^3	2	0.56	[47]
amorphous	3D- MSM array	8.9 (at 15V; spacing 10 μm)	10^3	1.5×10^{-5}	3×10^{-4}	[49]
ε*	Schottky MSM	230 (at 6V)	1.2×10^5	-	2.4×10^{-5}	[43]
ε*	Schottky MSM (Au)	0.52 (at 5V)	1.82×10^4	-	0.33	[44]
β	Schottky MSM (Ni/Au)	0.9 (at 5V)	7.8×10^4	< 1	< 3	[48]
β	Schottky MSM (Au)	96.13 (at 5V)	$>10^2$	3.2×10^{-2}	7.8×10^{-2}	[30]

* polymorph label cited in the reference (last column)

Conclusions

In summary, UV-C solar-blind photodetectors were fabricated from high-resistivity nominally-undoped n-type κ–Ga_2O_3 epilayers, and their spectral responsivity, rejection ratio (R_R) and ON-OFF inertia were extensively investigated.

Very high photo-gain was observed, linearly dependent on the applied bias up to a certain critical bias value. Beyond this voltage, the gain behavior departed from linear and finally reached a saturation at even higher applied bias. The high gain is explained in terms of excess of collected majority carriers (electrons) per unit time, possibly resulting from hole trapping/self-trapping in the conductive channel. An estimate of the minority carrier diffusion length was presented, based on the voltage value at which the photo-gain saturation occurs. This is the first estimate of the hole diffusion length in κ–Ga_2O_3.

The detectors subjected to ON-OFF illumination cycles with light at λ = 250 nm demonstrated high reproducibility and stability over long time. Time constants for ON and OFF transients were found to be comparable with literature data for UV photodetectors made with other Ga_2O_3 polymorphs. Tests with a solar simulator showed that the photodetectors exhibited negligible photocurrent under strong sunlight illumination, so that even a very weak UV-C radiation could easily be detected under contemporary sunlight exposure. As a matter of fact, a rejection ratio $R_S > 10^4$ and very high sensitivity make κ–Ga_2O_3 a suitable material for solar-blind UV-C photodetector.

Acknowledgements

The authors wish to thank Dr. Matteo Bosi and Dr. Luca Seravalli at IMEM-CNR Institute for providing the κ–Ga_2O_3 epilayers utilized in this work, and Dr. Piero Mazzolini at University of Parma for useful discussions.

Data availability

The raw data required to reproduce these findings cannot be shared at this time due to technical or time limitations. The data can however be requested to the authors at a later time.

References

[1] H. Chen, K. Liu, L. Hu, A. A. Al-Ghamdi and X. Fang, "New concept ultraviolet photodetectors vol. 18, no. 9, 2015," *Materials Today,* vol. 18, no. 9, 2015.

[2] E. Monroy, F. Omnés and F. Calle, "Wide-bandgap semiconductor ultraviolet photodetectors," *Semicond. Sci. Technol.,* vol. 18, no. R33-R51, 2003.

[3] C. Xie, X. T. Lu, X. W. Tong, Z. X. Zhang, F. X. Liang, L. Liang, L. B. Luo and Y. C. Wu, "Recent Progress in Solar-Blind Deep-Ultraviolet Photodetectors Based on Inorganic Ultrawide Bandgap Semiconductors," *Advanced Functional Materials,* vol. 29, p. 1806006, 2019.

[4] "Space Environment (Natural and Artificial) - Process for Determining Solar Irradiances.," *ISO 21348,* 2007.

[5] K. Osamura, K. Nakajima, Y. Murakami, P. H. Shingu and A. Ohtsuki, "Fundamental adsorption edge in GaN, InN and their alloys," *Solid State Commun.,* vol. 11, p. 617, 1972.

[6] X. Chen, H. Zhu, J. Cai and Z. Wu, "High-performance 4H-SiC based ultraviolet p-i-n photodetector," *J. Appl. Phys.,* vol. 102, p. 024505, 2007.

[7] J. D. Ye, S. L. Gu, S. M. Zhu, S. M. Liu, Y. D. Zheng, R. Zhang, Y. Shi, H. Q. Yu and Y. D. Ye, "Gallium doping dependence of single-crystal n-type ZnO grown by metal-organic chemical vapor deposition," *J. Cryst. Growth,* vol. 283, p. 279–85, 2005.

[8] C. D. J. Shao Z G, H. Lu, R. Zhang, D. P. Cao, W. J. Luo, Y. D. Zheng, L. Li and Z. H. Li, "High-Gain AlGaN Solar-blind Avalanche Photodiodes," *IEEE Electron Device Lett.,* vol. 35, p. 372–4, 2014.

[9] J. Yu, C. X. Shan, J. S. Liu, X. W. Zhang, B. H. Li and D. Z. Shen, "MgZnO avalanche photodetectors realized in Schottky structures," *Phys. Status Solidi RRL,* vol. 7, p. 425–8, 2013.

[10] W. Yang, S. S. Hullavarad, B. Nagaraj, I. Takeuchi, R. P. Sharma, T. Venkatesan, R. D. Vispute and H. Shen, "Compositionally-tuned epitaxial cubic MgxZn1-xO on Si(100) for deep ultraviolet photodetectors," *Appl. Phys. Lett.*, vol. 82, p. 3424–6, 2003.

[11] A. Cremades, M. Albrecht, J. Krinke, R. Dimitrov, M. Stutzmann and H. P. Strunk, "Effects of phase separation and decomposition on the minority carrier diffusion length in AlxGa1−x N films," *Journal of Applied Physics*, vol. 87, no. 5, pp. 2357-2362, 2000.

[12] S. J. Pearton, J. Yang, P. Cary, F. Ren, J. Kim, M. Tadjer and M. Mastro, "A review of Ga_2O_3 materials, processing and devices," *Appl. Phys. Rev*, vol. 5, p. 011301, 2018.

[13] A. Kuramata, A. Koshi, K. Watanabe, Y. Yamaoka, T. Masui and S. Yamakoshi, "High-quality β-Ga_2O_3 single crystals grown by edge-defined film-fed growth," *Jpn. J. Appl. Phys.*, vol. 55, 2016.

[14] P. Ravadgar, R.-H. Horng, S.-D. Yao, H.-Y. Lee, B.-R. Wu, S.-L. Ou and L.-W. Tu, "Effects of crystallinity and point defects on optoelectronic applications of β-Ga_2O_3 epilayers," *Opt. Express*, vol. 21, pp. 24599-24610, 2013.

[15] I. Cora, F. Mezzadri, F. Boschi, M. Bosi, M. Čaplovičová, G. Calestani and R. Fornari, "The real structure of ε-Ga_2O_3 and its relation to κ-phase," *CrystEngComm*, vol. 19, no. 11, pp. 1509-1516, 2017.

[16] R. Fornari, M. Pavesi, V. Montedoro, D. Klimm, F. Mezzadri, I. Cora, B. Pécz, F. Boschi, A. Parisini, A. Baraldi, C. Ferrari, E. Gombia and M. Bosi, "Thermal stability of ε-Ga_2O_3 polymorph," *Acta Materialia*, vol. 140, pp. 411-416, 2017.

[17] P. F. Chi, F. W. Lin, M. L. Lee and J. K. Sheu, "High-Responsivity Solar-Blind Photodetectors Formed by Ga_2O_3/p-GaN Bipolar Heterojunctions," *ACS Photonics*, vol. 9, no. 3, pp. 1002-1007, 2022.

[18] A. Parisini, A. Bosio, H. von Bardeleben, J. Jimenez, S. Dadgostar, M. Pavesi, A. Baraldi, S. Vantaggio and R. Fornari, "Deep and shallow electronic states associated to doping, contamination and intrinsic defects in epsilon Ga_2O_3 epilayers," *Materials Science in Semiconductor Processing*, vol. 138, p. 106307, 2022.

[19] A. Bosio, A. Parisini, A. Lamperti, C. Borelli, L. Fornasini, M. Bosi, I. Cora, Z. Fogarassy, B. Pécz, Z. Zolnai, A. Németh, S. Vantaggio and R. Fornari, "n-Type doping of ε-Ga_2O_3 epilayers by high-temperature tin diffusion," *Acta Materialia*, vol. 210, p. 116848, 2021.

[20] T. Makino, S. Yusa, D. Oka and T. Fukumura, "Temperature-dependent optical properties of ε-Ga_2O_3 thin films," *Japanese Journal of Applied Physics*, vol. 61, no. SB, p. SB1031, 2022.

[21] J. Li , Y. Zhou , X. Yi, M. Zhang , Y. Chen, M. Cui and F. Yan, "An Automatic Corona-discharge Detection System for Railways Based on Solar-Blind Ultraviolet Detection," *Current Optics and Photonics*, vol. 1, no. 3, pp. 196-202, 2017.

[22] T. Oshima, T. Okuno, A. Naoki, N. Suzuki, H. Hino and S. Fujita, "Flame Detection by a β-Ga_2O_3-Based Sensor," *Japanese Journal of Applied Physics*, vol. 48, p. 011605, 2009.

[23] M. Pavesi, F. Fabbri, F. Boschi, G. Piacentini, A. Baraldi, M. Bosi, E. Gombia, A. Parisini and R. Fornari, "ε-Ga_2O_3 epilayers as a material for solar-blind UV photodetectors," *Materials Chemistry and Physics*, vol. 205, pp. 502-507, 2018.

[24] F. Boschi, M. Bosi, T. Berzina, E. Buffagni, C. Ferrari and R. Fornari, "Hetero-epitaxy of Ga_2O_3 layers by MOCVD and ALD," *J. Cryst. Growth*, vol. 443, pp. 25-30, 2016.

[25] A. Bosio, C. Borelli, A. Parisini, M. Pavesi, S. Vantaggio and R. Fornari, "A Metal-Oxide Contact to ε-Ga_2O_3 Epitaxial Films and Relevant Conduction Mechanism," *ECS Journal of Solid State Science and Technology,* vol. 9, p. 055002, 2020.

[26] Z. Wang, X. Chen, F. Ren, S. Gu and J. Ye, "Deep-level defects in gallium oxide," *Journal of Physics D: Applied Physics,* 2020.

[27] D. Guo, Z. Wu, P. Li, Y. An, H. Liu, X. Guo, H. Yan, G. Wang, C. Sun, L. Li and W. Tang, "Fabrication of β- Ga_2O_3 thin films and solar-blind photodetectors by laser MBE technology," *Optical Materials Express,* vol. 4, pp. 1067-1076, 2014.

[28] X. Chen, F. Ren, S. Gu and J. Ye, "Review of gallium-oxide-based solar-blind ultraviolet photodetectors," *Photonics Research,* vol. 7, no. 4, pp. 381-415, 2019.

[29] R. H. Bube, Photoconductivity of Solids, Wiley & Sons, Inc, 1960.

[30] K. Arora, N. Goel, M. Kumar and M. Kumar, "Ultrahigh performance of self-powered β-Ga_2O_3 thin film solar-blind photodetector grown on cost-effective Si substrate using high-temperature seed layer," *ACS Photonics ,* vol. 5, p. 2391−2401, 2018.

[31] A. Parisini, A. Bosio, V. Montedoro, A. Gorreri, A. Lamperti, M. Bosi e R. Fornari, «Si and Sn doping of ε-Ga_2O_3 layers.,» *APL Materials,* vol. 7, n. 3, p. 031114, 2019.

[32] Y. Dan, X. Zhao, K. Chen and A. Mesli, "A photoconductor intrinsically has no gain," *Acs Photonics,* vol. 5, no. 10, pp. 4111-4116, 2018.

[33] A. V. Gert, A. P. Dmitriev, M. E. Levinshtein, V. S. Yuferev and J. W. Palmour, "Diffusion of minority carriers against electric field (high injection level)," *Applied Physics Letters,* vol. 20, no. 111, p. 203503, 2017.

[34] J. L. Lyons, "Electronic properties of Ga_2O_3 polymorphs," *ECS Journal of Solid State Science and Technology,* vol. 8, no. 7, p. Q3226, 2019.

[35] E. B. Yakimov, A. Y. Polyakov, N. B. Smirnov, I. V. Shchemerov, P. S. Vergeles, E. E. Yakimov, A. Chernykh, X. M, F. Ren and S. J. Pearton, "Role of hole trapping by deep acceptors in electron-beam-induced current measurements in β-Ga_2O_3 vertical rectifiers," *Journal of Physics D: Applied Physics,* vol. 53, no. 49, p. 495108, 2020.

[36] A. M. Armstrong, M. H. Crawford, A. Jayawardena, A. Ahyi and S. Dhar, "Role of self-trapped holes in the photoconductive gain of β-gallium oxide Schottky diodes," *Journal of Applied Physics,,* vol. 119, no. 10, p. 103102, 2016.

[37] E. B. Yakimov, A. Y. Polyakov, N. B. Smirnov, I. V. Shchemerov, J. Yang, F. Ren, G. Yang, J. Kim and S. J. Pearton, "Diffusion length of non-equilibrium minority charge carriers in β-Ga_2O_3 measured by electron beam induced current," *Journal of Applied Physics,* vol. 123, no. 18, 2018.

[38] A. Parisini, K. Ghosh, U. Singisetti and R. Fornari, " Assessment of phonon scattering-related mobility in β-Ga_2O_3," *Semiconductor Science and Technology,* vol. 33, no. 10, p. 105008, 2018.

[39] M. Mulazzi, F. Reichmann, A. Becker, W. M. Klesse, P. Alippi, V. Fiorentini, A. Parisini, M. Bosi and R. Fornari, "The electronic structure of ε-Ga_2O_3," *APL Materials,* vol. 7, no. 2, p. 022522, 2019.

[40] H. J. Von Bardeleben, J. L. Cantin, A. Parisini, A. Bosio and R. Fornari, "Conduction mechanism and shallow donor properties in silicon-doped ε-Ga_2O_3 thin films: An electron paramagnetic resonance study," *Physical Review Materials,* vol. 3, no. 8, p. 0846, 2019.

[41] F. Akyol, "Simulation of β-Ga_2O_3 vertical Schottky diode based photodetectors revealing average hole mobility of 20 cm2 V-1 s-1," *Journal of Applied Physics,* vol. 127, no. 7, p. 074501, 2020.

[42] J. B. Varley, A. Janotti, C. Franchini and C. G. Van de Walle, "Role of self-trapping in luminescence and p-type conductivity of wide-band-gap oxides," *Physical Review B,* vol. 85, no. 8, p. 081109, 2012.

[43] Y. Qin, L. Li, X. Zhao, G. S. Tompa, H. Dong, G. Jian, Q. He, P. Tan, X. Hou, Z. Zhang, S. Yu, H. Sun, G. Xu, X. Miao, K. Xue, S. Long and M. Liu, "Metal–semiconductor–metal ε-Ga_2O_3 solar-blind Photodetectors with a record-high responsivity rejection ratio and their gain mechanism," *ACS Photonics,* vol. 7, no. 3, pp. 812-820, 2020.

[44] Z. Liu, Y. Huang, C. Zhang, J. Wang, H. Li, Z. Wu, P. Li and W. Tang, "Fabrication of epsilon-Ga_2O_3 solar-blind photodetector with symmetric interdigital Schottky contacts responding to low intensity light signal," *Journal of Physics D: Applied Physics,* vol. 53, no. 29, 2020.

[45] X. Liu, P. Guo, T. Sheng, L. Qian, W. Zhang and Y. Li, "β-Ga_2O_3 thin films on sapphire pre-seeded by homo-self-templated buffer layer for solar-blind UV photodetector," *Optical Materials,* vol. 51, pp. 203-207, 2016.

[46] L. X. Qian, H. Y. Liu, H. F. Zhang, Z. H. Wu and W. L. Zhang, "Simultaneously improved sensitivity and response speed of beta-Ga_2O_3 solar-blind photodetector via localized tuning of oxygen deficiency," *Applied Physics Letters,* vol. 114, p. 113506, 2019.

[47] L.-X. Qian, H.-F. Zhang, P. T. Lai, Z.-H. Wu and X.-Z. Liu, "High-sensitivity β-Ga_2O_3 solar-blind photodetector on high-temperature pretreated c-plane sapphire substrate," *Optical Materials Express,* vol. 7, pp. 3643-3653, 2017.

[48] F. P. Yu, S. L. Ou and D. S. Wuu, "Pulsed laser deposition of gallium oxide films for high performance solar-blind photodetectors," *Optical Materials Express,* vol. 5, pp. 1240-1249, 2015.

[49] Y. Chen, Y. Lu, M. Liao, Y. Tian, Q. Liu, C. Gao, X. Yang and C. Shan, "3D Solar-Blind Ga_2O_3 Photodetector Array Realized Via Origami Method," *Advanced Functional Materials,* p. 1906040, 2019.